Journal of Hazardous Materials, 24 (1990) 39–65
Elsevier Science Publishers B.V., Amsterdam — Printed in The Netherlands

DISPERSION OF A DENSE CYLINDRICAL CLOUD IN CALM AIR

C.S. MATTHIAS

Atmospheric Environment Service, 4905 Dufferin Street, Downsview, Ontario M3H 5T4 (Canada)

(Received June 1, 1989; accepted in revised form February 10, 1990)

Summary

A simple analytical semi-empirical model is presented which describes the concentration field in a collapsing gas cloud of cylindrical shape. The model examines the processes of top and side entrainment, the occurrence of a leading torus and a trailing disk, and Gaussian distributions in the entrainment zones. These processes are described for cases in which there are no atmospheric effects, i.e., no wind or ambient turbulence. Turbulence within the cloud is self-generated, due to the sudden collapse of the cloud. The model contains several universal constants which are evaluated using data from a laboratory study carried out at the University of Arkansas. The model is then compared to results from a laboratory study at the Colorado State University and a full scale 2000 m^3 release of freon at Thorney Island. The initial cloud volumes of these laboratory and field studies encompass a range of eight orders of magnitude.

1. Introduction

In the past decade, there has been intense effort to gain an improved understanding of the process of dense gas dispersion. Stimuli have come from several disastrous spills of gases and liquids, as well as from the need to predict with some confidence the hazard zones associated with production, transport, and storage of chemicals. Dense gas behaviour is not well described by the frequently used Gaussian dispersion models. A Gaussian model provides a reasonable description of the concentration distribution within a puff or plume of neutral or positive buoyancy. For a gas which has negative buoyancy by virtue of high molecular weight, low temperature, or suspended aerosols, the vertical growth rate is reduced and the lateral growth rate is enhanced. A low flat cloud is generated and remains so until the cloud density is close enough to ambient air density such that ambient turbulence can penetrate and control the cloud growth.

Several models have been developed to describe instantaneous spills. Their characteristics are described and compared in a comprehensive review by Wheatley and Webber [1]. The variety of models, both analytical and numerical, suggests the following deficiencies in our understanding of dense gas be-

0304-3894/90/$03.50

haviour: (1) there are several different expressions for top entrainment and for edge entrainment (2) there is no consensus as to whether top or edge entrainment is more important or whether there should even be any distinction between the two (3) there are several criteria for determining the means by which gravitationally controlled entrainment yields to entrainment by ambient turbulence (4) there is inadequate model evaluation (5) concentration estimates may differ by an order of magnitude.

Most model development has concentrated on cylindrical box models which attempt to describe bulk or mean properties, such as radius, height, and concentration, for the dispersing cloud. One of the earliest dense gas box models for application in a windless environment was that of Van Ulden [2] incorporating side entrainment only. Another early model by Germeles and Drake [3] had only top entrainment. In both of these models, the entrainment velocity was assumed to be proportional to the radial expansion velocity. Fay [4] employed the above entrainment schemes simultaneously and deduced the edge entrainment to be negligible. He further modified the model for application in non-zero winds and calibrated it using several field and wind tunnel studies. In a later paper [5], Fay and Ranck criticized the above entrainment model which allowed the cloud height to grow indefinitely, thus violating the law of conservation of energy. In a more recent study, Fay and Zemba [6] abandon the previous entrainment concept and use an empirical model for concentration decay based upon concentration observations and upon cloud height observations where the cloud height remains fairly constant in time.

Models such as these are simple enough to integrate analytically. The next step in complexity is to improve the physics within the box model structure such that a numerical solution is required, with time still being the sole independent variable. One such by Webber and Wheatley [7] employs equations for the conservation of mass, momentum, and turbulent energy (TE). The model is structured as a top entrainment model, in which the entrainment rate is controlled by the TE and a TE Richardson number. However, they conclude that top entrainment need not be considered in calm conditions and that the traditional simple edge entrainment model produces the correct concentration decay. At a IUTAM symposium, a paper by Van Ulden [8] described a complex box model for the 2-dimensional spread of a finite release. In accordance with the frequently observed feature of a distinct leading head followed by a longer lower tail, the model examines the properties of both, using the conservation equations for matter and momentum. In later publications [9,10], Van Ulden modifies the equations and adds an equation for the evolution of turbulent kinetic energy. A basic assumption, based on observations, is that edge entrainment is negligible.

The purpose of a model is to describe a physical process such that the model physics and the solution accuracy are reasonable. There is sufficient conflict and uncertainty in the literature to justify other attempts at describing con-

centration decay during the early stages of gravitational collapse. We will look primarily for dominant processes and simple analytical solutions where possible, since these convey the greatest understanding and most compact presentation in terms of non-dimensional plots.

The aim of this paper is to develop, calibrate, and evaluate a simple analytical heavy gas model to predict gas concentrations following an instantaneous release in a calm environment. The release begins as a uniform cylinder of gas at time zero. A cylindrical model is appropriate, since all gas or volatile liquid spills of short duration quickly develop quasi-cylindrical symmetry. Dilution occurs continuously as air is entrained through the top and side. A cylindrical model is particularly appropriate for comparison with several laboratory and field experiments which examined the collapse of a uniform cylinder of gas.

In the first few seconds, the cylinder height decreases and radius increases, with relatively little change in the cylinder volume. As entrainment of ambient air begins and continues, the height is determined by the difference between vertical entrainment and gravitational collapse. Experimental results usually show that the cylinder differentiates into two distinct bodies – a leading torus and a trailing disk. The properties of each are interesting and both are examined in the following model development.

We also hope to gain a better understanding of the early processes of cloud growth which are controlled by gravitational forces alone. This is most easily done by examining a data set in which there is no wind or external turbulence. When these processes are understood and parameterized, they can be included later in a more general atmospheric entrainment model.

The concentration model is an axisymmetric hybrid box model (Fig. 1). It is a function of independent variables z (height), r (radius), and t (time). The leading torus extends to a radius R_f (frontal radius) and has a rectangular

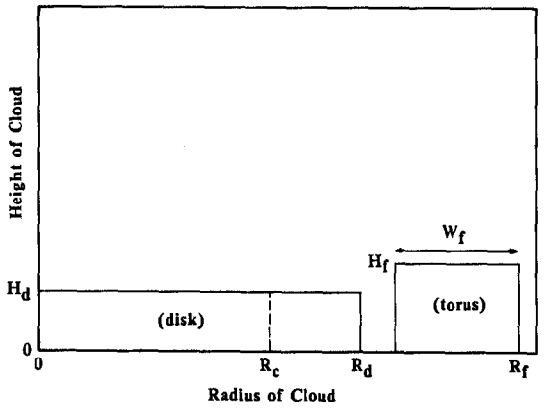

Fig. 1. Bulk model schematic of an expanding cylindrical dense gas cloud as it differentiates into a disk and a torus.

cross-section of width W_f and height H_f. The trailing disk has a radius R_d and a height H_d. Although the torus and disk in reality interact with each other, they can be modelled separately to a first approximation. Entrainment of air is assumed to occur through the top and sides of each body. Each body is treated as a box model in order to calculate a maximum concentration.

The use of bulk or box models serves several purposes. They identify the major processes, establish characteristic dimensions, give reasonable maximum values, and are simple to derive and to solve. To these solutions are attached Gaussian profiles to describe the decrease in concentration due to entrainment of air at the top and at the edges. The Gaussian was selected as a trial distribution because of its familiarity and for its mathematical convenience. (It also allows a smooth transition to a Gaussian distribution resulting from dispersion by atmospheric turbulence as the dense puff becomes neutral.) The primary requirements on the part of the model are that mass is conserved, that the equations of motion and of entrainment are universal, and that the solutions agree with the data.

The model is its present form is of limited application, since ambient atmospheric turbulence is assumed to be zero. The model may, however, be applicable in the early stages of cloud growth in the atmosphere during which self-induced turbulence is dominant. This allows it to be applied to the dispersion of dense flammable gases in which a hazard exists only for concentrations exceeding 1% by volume.

The data which are used to calibrate and evaluate the model were generated in a laboratory study by Havens and Spicer [11]. In the study, a right circular cylinder of freon and air was instantaneously released. The initial volumes were 34, 54, 135, and 535 litres; initial specific gravities were 2.16, 2.91, and 4.19; initial height/diameter ratios were 0.4, 1.0, and 1.57. Concentration time series were measured at several vertical and radial positions from the spill centre. A total of 67 experiments were reported, each having measurements at 8 receptors. By plotting in suitable non-dimensional coordinates, the authors show the concentration decay within the drifting cloud (Lagrangian mode) to be similar to that of the Thorney Island experiments. The latter are full scale studies and employ initial freon–air mixtures of 2000 m^3 [12].

Each time series graph [11] contains results of 2 or 3 trials for identical initial conditions and so gives some idea of the variability within each experiment. For each trial, the data of specific interest to Havens and Spicer were the peak concentration, its time of arrival, and the time of arrival of the cloud front. As shown in their report [11], the peaks were not random fluctuations but were distinct and repeatable properties of the expanding cloud.

Two typical time series from Havens and Spicer [11] are shown in Fig. 2. This sensor was located 2.0 m from the centre of the release point. In Fig. 2(a), the concentration was measured at a height of 0.6 cm. Following the peak concentration, there is a strong dip and then a rise to a second maximum. The dip

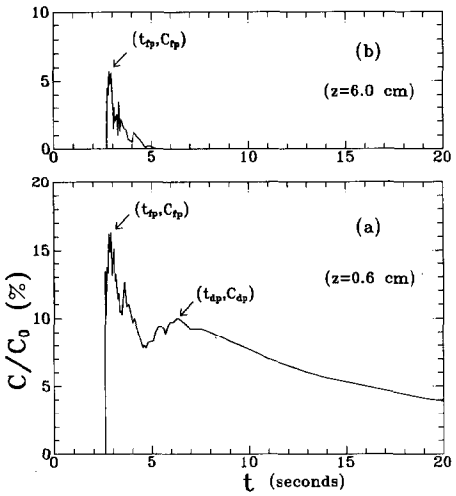

Fig. 2. Measured concentrations vs. time at two different receptor elevations at a radius of 2 metres (Eulerian mode). Initial conditions: $V_o = 54.1$ litres, $\rho_o/\rho_a = 4.19$, $H_o/D_o = 1.0$ (from Havens and Spicer [11]).

seems to mark the passage of the torus. The concentration curve measured at a height of 6 cm (Fig. 2b) marks the arrival and departure of the torus, but sees very little of the trailing cloud which must be significantly lower.

The present model development explores the roles of both the frontal torus and the trailing disk. From the laboratory time series [11], we have abstracted 5 data; time of arrival (t_a) of the front, time of several (t_{fp}) of the frontal peak concentration (C_{fp}), and time of arrival (t_{dp}) of the disk peak concentration (C_{dp}). (The latter two data are not measurable at the higher monitors.) The data are selected at various radii from the release point and at various heights above the laboratory floor. Uncertainties in the disk data are larger, since the division between disk and torus is not always distinct and undulations in the data are sometimes large.

In addition, data from other zero wind experiments are compared with the model results. The comparison is most interesting using experiments which differ significantly from those of Havens and Spicer. In other studies, the only parameter which is significantly different is the initial volume of gas V_o. The laboratory studies of Meroney and Lohmeyer [13] use three values of V_o: 0.035, 0.165, and 0.45 litres. The full scale Thorney Island experiments [12] release a gas volume of 2 million litres into the atmosphere. These two studies provide a range of 8 orders of magnitude in V_o for comparison to the model and to the Havens and Spicer data. Plots of concentration histories and isolines from two other laboratory studies [14,15] were briefly examined but were not used. Their results were comparable to the previously mentioned studies.

TABLE 1

Initial conditions and characteristic numbers for each release

Ref.	V_o (litres)	ρ_o/ρ_a	H_o/D_o	l eqn.(6) (cm)	τ eqn.(7) (s)	$\bar{t}_{r_*}$ eqn.(10) (Model 1)
	34.2	4.19	1.0	32.5	0.10	2760
	54.1	4.19	1.0	37.8	0.11	3470
	135	4.19	1.0	51.3	0.13	5480
	535	4.19	1.0	81.2	0.16	10910
Havens	34.2	2.91	1.0	32.5	0.10	2130
and	54.1	2.91	1.0	37.8	0.11	2680
Spicer	34.2	2.16	1.0	32.5	0.10	1660
	135	2.91	1.0	51.3	0.13	4240
	135	2.16	1.0	51.3	0.13	3310
	54.1	4.19	0.4	37.8	0.11	3470
	54.1	4.19	1.57	37.8	0.11	3470
Meroney	0.035	4.19	0.5	3.3	0.032	90
and	0.165	4.19	0.5	5.5	0.042	190
Lohmeyer	0.450	4.19	0.5	7.7	0.050	315
McQuaid	2×10^6	1.6	0.93	1260	1.46	290000

Initial conditions for all releases are given in Table 1. The characteristic dimensions in the table are explained later.

2. Radial growth

2.1 The conventional model

As a gravity-driven intrusion spreads, it maintains a distinct front for some time. This front corresponds to the leading edge of the torus as discussed in the introduction. In this section on radial growth, we will not distinguish between torus and disk. The cloud is treated as a uniform cylinder having radius R, volume V, and height H. We are interested in developing and calibrating an expression for the radius R of the outermost edge of the cloud as it expands as a function of time.

Analyses of virtually all experimental studies of dense collapsing gas clouds show that the radial growth is proportional to the square root of time. The driving force is created by the pressure of the negatively buoyant fluid. The resulting force may be a combination of terms. A suitable model can be derived if one assumes a quasi-equilibrium, i.e., an approximate balance between the pressure head of the dense gas and the form drag on the expanding rim [16].

The same model arises by balancing the pressure head against the inertial force [17]. The conventional model for radial growth of a uniform cylinder is shown to be

$$\frac{dR}{dt}=a_1(gH\Delta)^{1/2}=a_1 b^{1/2}/R \tag{1}$$

where

$$b=gV\Delta/\pi \tag{2}$$

$$\Delta=(\rho-\rho_a)/\rho_a \tag{3}$$

In these equations, t is time elapsed, g is the gravitational constant, ρ and ρ_a are the densities of the dense gas and of air respectively, and a_1 is a proportionally constant. As the cloud grows and entrains air, V grows while the relative density excess Δ decreases. It is shown in [16] that b is conserved for (i) isothermal flows and (ii) nonisothermal flows in which the gas and air molar specific heats are equal and for which ground heating is negligible. This allows eqn. (1) to provide a robust description of a large class of density driven motion, the solution for which is

$$R^2=R_o^2+2a_1 b_o^{1/2}t \tag{4}$$

where R_o is the initial radius of the cylindrical cloud, and b_o is the initial buoyancy given by

$$b_o=gV_o\Delta_o/\pi \tag{5}$$

If eqn. (4) is rewritten in nondimensional form using the length and time scales suggested by Fay [4], where

$$l=V_o^{1/3} \tag{6}$$

and

$$\tau=(l/g\Delta_o)^{1/2} \tag{7}$$

then

$$\bar{R}^2-\bar{R}_o^2=2a_1\bar{t}/\pi^{1/2} \tag{8}$$

where $\bar{R}=R/l$, $\bar{R}_o=R_o/l$, and $\bar{t}=t/\tau$. Equation (8) implies that an appropriate nondimensional plot of cloud radius measurements versus time in logarithmic coordinates should collapse along a single straight line. The data of Havens and Spicer [11] corroborate this in Fig. 3. In this figure, there is a linear portion in the range $20<\bar{t}<100$ to which eqn. (8) can be applied. The best value for the calibration constant is found to be $a_1=1.16$ which is in good agreement with the generally accepted values of 1.1 ± 0.1 as determined from a large number of field and laboratory experiments [18]. Equation (8) is plotted in Fig. 3. If we designate the modelled values of R as R_{mod} and the observed values as

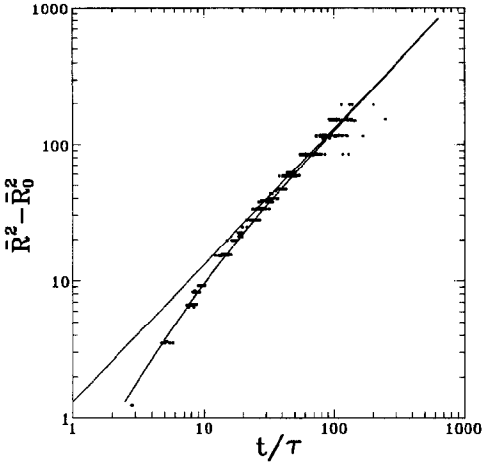

Fig. 3. Location of the cloud leading edge as a function of time. Upper solid curve from eqn. (8): lower solid curve from eqn. (12); ● data from Havens and Spicer [11].

R_{obs}, then the mean and standard deviation of R_{mod}/R_{obs} are 1.02 ± 0.053 in the range $20 < \bar{t} < 100$.

For $\bar{t} > 100$, there is increased scatter in locating the position of the frontal edge of the cloud. This is due to several factors: (1) the signal is weak (2) the signal is diffuse rather than sharp (3) the effect of variability between runs increases with distance (4) the presence of the laboratory walls may have an effect (5) the balance of forces acting on the cloud may change with time such that R^2 no longer grows as t.

The data of Fig. 3 hint that the R^2 growth may be slowing down significantly for large time. A review by Simpson [19] states that if the buoyancy–inertia balance of forces gives way to a buoyancy–viscous balance, R will change from a $t^{0.5}$ growth to a $t^{0.25}$ growth. The time at which this transition occurs is given by

$$t_* = (V/\nu g \Delta)^{1/3} \tag{9}$$

where ν is the viscosity of the fluid. This expression has been successfully compared with data but only for experiments in which V and Δ remained constant. It can be modified to use a mean value of V and Δ for application to an entraining dense gas cloud. Recalling that $V\Delta = V_o \Delta_o$, and borrowing the asymptotic value for cloud volume from eqn. (25), eqn. (9) can be written in non-dimensional form as

$$\bar{t}_{r_*} = \left[\frac{c_1^{2c_2}}{\nu}(g V_o \Delta_o)^{1/2}\right]^{1/(3-4c_2)} \tag{10}$$

The Havens and Spicer experiments which produce the smallest t_{r_*} have $V_o = 34$

litres and $\rho_o/\rho_a=2.16$ (see Table 1). Taking an air viscosity of 1.5×10^{-5} m^2 s^{-1}, we find that $\bar{t}_{r_v}=1660$. This is the non-dimensional time at which viscous effects should begin to affect the radial growth. This time is well beyond the range of the Havens and Spicer experiments.

2.2 Initial acceleration

In Section 2.1, it was mentioned that eqn. (4) resulted from a quasi-equilibrium of forces. When the cylinder is released, however, there must be a period of acceleration from rest. The acceleration zone is quite evident in Fig. (3) for nondimensional times less than 15. It is somewhat fortuitous that the data cling to a single line, implying that the curve is universal. If so, we can derive a kinematic relationship between R and t without describing the dynamics of the problem. Since the slope of the curve for small time appears to be 2, an appropriate asymptotic form of the curve near $t=0$ is

$$\bar{R}^2-\bar{R}_o^2=a_4\bar{t}^2 \qquad (\bar{t}\ll 10) \tag{11}$$

This expression is physically realistic since for $t=0$, the velocity is zero and the acceleration is positive and decreasing. Blending eqns. (8) and (11), we have a general expression for the location R_f of the leading or frontal edge of the cloud given by

$$\bar{R}_f^2-\bar{R}_0^2=\frac{2a_1a_4\bar{t}^2}{2a_1+a_4\pi^{1/2}\bar{t}} \tag{12}$$

Retaining the former parameter value of $a_1=1.16$, eqn. (12) makes a good fit with the data if the new acceleration parameter is chosen as $a_4=0.35$. The mean and standard deviation of R_{mod}/R_{obs} are 1.01 ± 0.042 for $1<\bar{t}<20$, and 0.97 ± 0.047 for $20<\bar{t}<100$. Equation (12) is plotted in Fig. 3. By equating the two terms of the denominator of eqn. (12), we find that the acceleration period gives way to the quasi-equilibrium period at a time $t\simeq4\tau$. This implies that the characteristic time τ given by eqn. (7) is a measure of the period of initial acceleration of the expanding cloud front.

3. Entrainment

Entrainment is the process by which ambient air is captured at the cloud boundaries and is mixed into the cloud. Several experimental studies have been done to examine the process and are reviewed by Simpson [20].

In this review, there is a great deal of photographic evidence from both gas and liquid flow studies to show that many gravity flows have a distinct head at the leading edge. The head is the region of intense turbulence generation and mixing. Most 2-dimensional laboratory studies examine a stationary hydraulic flow balanced by an opposing wind field. The flow is complex, with fluid moving from the tail along the floor into the head, and returning along the top

surface of the tail. Turbulence may consist of large organized waves, or lobes, or may be diffuse. It is generally more vigorous over the head than over the tail.

In our application, we are concerned with a sudden cylindrical expansion into a calm atmosphere. The maximum concentration torus and disk data that were abstracted from the concentration vs. time curves at each receptor [11] indicates that the torus concentration falls off as $t^{-1.5}$ (Fig. 8) whereas the disk concentration falls off as $t^{-1.0}$ (Fig. 4). This is in keeping with the observation that the turbulence, and hence entrainment, is more vigorous in the torus than in the disk.

A box model serves to describe the temporal behaviour of a characteristic or significant concentration which we shall take as the maximum concentration. Since a box model concentration is uniform, an implicit assumption is that entrained air is mixed rapidly throughout the box. Experimental results will resemble box model results only if there is adequate mixing in reality. We are interested in separate box models for the disk and for the torus.

Initially, we examine the possible entrainment mechanisms into the disk or the torus. Virtually all cylindrical box models begin with the equation

$$\frac{\mathrm{d}V}{\mathrm{d}t}=\pi R^2 v_\mathrm{t}+2\pi RHv_\mathrm{e} \tag{13}$$

where v_t and v_e are the top and edge entrainment rates respectively. Similarly, top entrainment into a torus can be described by $2\pi RWv_\mathrm{t}$ where the torus width $W \ll R$. Note that the structure of eqn. (13) also serves to describe entrainment into the torus provides that $W \propto R$. Traditionally it has been felt that on the edge, there was vigorous entrainment acting upon a small area whereas on top, there was weak entrainment acting upon a large area. Hence there was a possibility of comparable net entrainment on each surface. If we assume that the entrainment velocity is proportional to the radial expansion speed, eqn. (13) can be integrated exactly [4]. However, the entrainment process can be examined more clearly if we assume either top or edge entrainment to be dominant.

Since entrainment and cloud turbulence are closely linked, it is instructive to examine the total rate of change of turbulence energy (TE) equation given by Mellor and Yamada [21]:

$$\frac{\partial q^2}{\partial t}+U_\mathrm{k}\frac{\partial q^2}{\partial x_\mathrm{k}}=-2\overline{u_\mathrm{k}u_\mathrm{i}}\frac{\partial U_\mathrm{i}}{\partial x_\mathrm{k}}+\frac{\partial}{\partial x_\mathrm{k}}\left[\tfrac{5}{3}q\lambda\frac{\partial q^2}{\partial x_\mathrm{k}}\right] -2\beta g_\mathrm{k}\overline{u_\mathrm{k}\theta}-2\frac{q^3}{\Lambda} \tag{14}$$

where $q^2=\overline{u_\mathrm{k}^2}$, λ and Λ are turbulence length scales, and u_i and U_i are scalar components of the turbulent and mean velocities respectively. The total rate of change of TE is controlled by the relative contributions of, from left to right,

shear production, dispersion, buoyancy work, and dissipation on the right hand side of eqn. (14). Since the height to width ratio rapidly becomes small in a collapsing cloud, the vertical gradients become dominant. When applied to an unsteady non-advecting box, eqn. (14) can be simplified (by using the equations of Section 2) to become

$$\frac{dq^2}{dt}=\frac{b_1q^2U}{H}-\frac{b_2q^3}{H}-\frac{b_3gq\Delta_oV_o}{V}-\frac{b_4q^3}{H} \tag{15}$$

Neglecting side entrainment for the moment, volume growth due to top entrainment is described by

$$\frac{dV}{dt}=\pi R^2v_t \tag{16}$$

where $v_t=b_5q$, b_1 to b_5 are universal calibration constants, and $U=dR/dt$. In our search for simple solutions (which are suggested by the near linear concentration decay in the log–log plots of Figs. 4 and 8), we assume that $q\propto t^n$. Since $R\propto t^{0.5}$, eqn. (16) integrates to give $V\propto t^{n+2}$ from which $H\propto VR^{-2}\propto t^{n+1}$. The time dependence of all terms in eqn. (15) can now be evaluated.

If we assume that a quasi-equilibrium exists between shear production and one of the decay terms of eqn. (15), dimensional analysis shows that $n=-0.5$. This implies that $V\propto t^{1.5}$, $H\propto t^{0.5}$, and $C\propto t^{-1.5}$. This behaviour is not supported by the disk data but is supported by the torus data. Furthermore, the analysis is also applicable to the torus since top entrainment described by eqn. (16) is equivalent to top entrainment into the torus provided that the torus width is proportional to R. Assuming a quasi-equilibrium between the shear term and any decay term of eqn. (15), we find that $q\propto U$ (radial expansion speed). This relationship has been assumed in many box models.

If we assume that there is not enough shear to support a quasi-equilibrium, then the TE decays in proportion to the remaining terms on the right side of eqn. (15). For this assumption of unsteady decay and negligible shear, the results apply only to the disk, where shear may be small. If the decay is due to buoyant work done by the cloud, we find again that $n=-0.5$ which leads to disagreement with the disk data. On the other hand, if the TE decay is due to either diffusion or dissipation, then n is undefined and may take any reasonable value. Hence, it is possible to choose a value of n to suit the disk concentration decay data once eqns. (15) and (16) are integrated. This analysis suggests that there is no ongoing turbulence generation in the disk as the TE decays, and that $n=-1.0$ may be chosen to fit the data.

A similar analysis can be done for edge entrainment, by replacing the right side of eqn. (16) with $2\pi RHv_e$ where $v_e=b_6q$, and b_6 is a constant. A more restricted set of solutions is available and allows only a single value of n, i.e.,

$n = -0.5$. If shear-generated turbulence is assumed to be important (a reasonable assumption for the edge of the expanding cylinder), then the concentration decays as $C \propto t^{-b}$, where b is an arbitrary constant. However, b is the only adjustable parameter and by itself is not sufficient to force the solution through the data. The top entrainment scheme allows for two adjustable parameters which are sufficient to fit the data.

In summary, the above analysis suggests that top entrainment is dominant over side entrainment in its effect upon both disk and torus. Within the torus, shear-generated turbulence is balanced by any or all of the decay terms. Within the disk, there is insufficient shear to maintain turbulence and the initial value decays rapidly. The initial value is presumably created by the sudden collapse of the compact cylinder. This description is in keeping with experimental observations which show the head of a gravity current to be more active than the tail.

Intuitively, side entrainment is unlikely to be able to penetrate to the central portion of the cloud as the cloud is expanding. The radial growth rate into the disk (or into the torus) is proportional to the torus turbulence and hence to the expansion velocity U. Therefore, the entrainment zone grows inward in proportion to R_f as the gravitational expansion grows outward in proportion to R_f, the latter being larger. Although it does not influence the maximum concentration, the lateral diffusion is retained as a mechanism for generating lateral decaying "wings" on the disk and torus bodies. Vertical diffusion through the relatively thin bodies immediately establishes a concentration profile that decays with height.

In the following two Sections, equations are developed for the time variation of the bulk concentrations of the disk and torus. The concentration of most interest is the maximum concentration. Hence in calibrating the model, the bulk concentration will be equated with the maximum, i.e., $C_{db} = C_{dp}$ and $C_{fb} = C_{fp}$.

4. The disk box model

Following the collapse of a compact cylindrical cloud, we assume that it splits immediately into a disk and a torus. During the initial collapse, a portion f of the initial potential energy PE_o is converted to initial turbulent energy TE_o within the disk where these are given by [9]

$$PE_o = \rho_a g V_o \Delta_o H_o / 2 \tag{17}$$

$$TE_o = \rho V_o q_o^2 / 2 \tag{18}$$

and

$$f = TE_o / PE_o \tag{19}$$

Assuming that further turbulence generation within the disk is negligible, and that the initial turbulence decays by viscous dissipation, eqns. (15) and (16) can be applied to the disk as

$$\frac{dq^2}{dt} = -\frac{b_4 q^3}{H_d} \tag{20}$$

and

$$\frac{dV_d}{dt} = \pi R_d^2 b_5 q \tag{21}$$

Since $V_d = \pi R_d^2 H_d$, these can be integrated to become

$$(q/q_o)^2 = \left(\frac{V_d}{V_o}\right)^{-b_4/b_5} \tag{22}$$

and

$$\frac{V_d}{V_o} = (1 + (2b_5 + b_4)\frac{\pi^{1/2} a_1}{2}\frac{q_o \tau}{l}\bar{t}^2)^{2b_5/(2b_5+b_4)} \tag{23}$$

For mathematical convenience, we ignore the existence of the torus and assume that the initial volume of the disk is the total initial volume V_o. This is true initially, and for very large times after the disk has absorbed the torus. Using eqns. (17–19), the initial turbulence within the disk can be expressed as a function of the initial aspect ratio H_o/D_o

$$\left(\frac{q_o \tau}{l}\right)^2 = f\left(\frac{4}{\pi}\right)^{1/3}\left(\frac{H_o}{D_o}\right)^{2/3} \tag{24}$$

Inserting this into eqn. (23), and regrouping the constants, the general expression for the bulk volume growth of the disk becomes

$$\bar{V}_d = \frac{V_d}{V_o} = \left(1 + c_1\left(\frac{H_o}{D_o}\right)^{1/3}\bar{t}^2\right)^{c_2} \tag{25}$$

where the universal constants c_1 and c_2 are chosen such that the bulk concentrations C_{db} match the peak concentrations C_{dp}. The bulk concentration is given by

$$\bar{C}_{db} = C_{db}/C_o = V_o/V_d \tag{26}$$

where C_o is the initial gas concentration. These equations are sufficient to characterize the time decay of the disk concentration. In order to characterize the radius R_d, we choose an empirical expression which allows the radius to be R_o initially and proportional to R_f at later times, i.e.,

$$\bar{R}_d^2 - \bar{R}_o^2 = a_7^2(\bar{R}_f^2 - \bar{R}_o^2) \tag{27}$$

where a_7 will be determined later. The height of the disk associated with gravitational slumping and turbulent entrainment is then expressed as

$$\bar{H}_d = H_d/l = \bar{V}_d/\pi\bar{R}_d^2 \tag{28}$$

The calibration constants c_1 and c_2 were chosen by comparing the modelled concentration eqn. (26) with the observed peak concentrations of Havens and Spicer [11] using the statistics $r = C_{mod}/C_{obs}$ and $\log r$. For values of $c_1 = 0.040$ and $c_2 = 0.5$, the mean and standard deviation (SD) of r are 1.04 ± 0.31 over the full range of data. The data and the theory (model 1) for three values of H_o/D_o are shown in Fig. 4. (Model 2 differs from model 1 primarily in the choice of disk parameters c_1, c_2, and a_7 and will be discussed in Section 8.) The importance of the aspect ratio in eqn. (25) could not be ascertained. When H_o/D_o was eliminated from the equation, the standard deviation was virtually unchanged. Although the aspect ratio ranged from 0.4 to 1.57, uncertainty in the data may have masked the influence of H_o/D_o.

A knowledge of the mean and standard deviation of r (or $\log r$) allows us to characterize the uncertainty of applying the model to a comparable problem. The uncertainty would be less well known if applied to an alternate problem with significantly different initial conditions. The four factors which contribute to uncertainty are (1) errors in model physics, (2) errors in model inputs, (3) errors in observations, and (4) inherent uncertainty [22]. In the present laboratory application, errors (2) and (3) are minimal, since environmental conditions and measurement locations are controlled. Inherent uncertainty arises due to random or turbulent processes over which we have no control. A

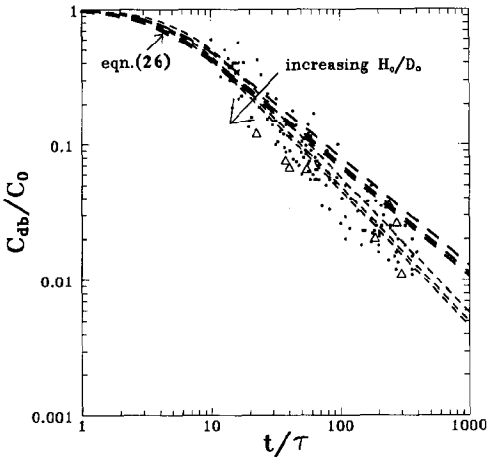

Fig. 4. The decay of the near-surface core concentration as the disk expands about the point of release: $H_o/D_o = 0.4$, 1.0, 1.57 (Lagrangian mode). --- Model 1; - - Model 2; ● data from Havens and Spicer [11]; △ Thorney Island No. 9 experiment.

qualitative picture of inherent uncertainty is presented in several references in which traces of concentration vs. time are superimposed for identical initial conditions [11,23,24].

The parameter a_7 is used to adjust the size of R_d relative to R_f. Since measurements of R_d are not available, a_7 cannot be evaluated directly from eqn. (27). However, it can be evaluated through the use of eqn. (28). In the following Section, the concentration distribution as a function of height z and disk height H_d is examined. The parameter a_7 is chosen so that the modelled distribution fits the measured distribution.

A model which is calibrated to a data set and which reproduces its behaviour with a small SD is a good model, assuming that it contains relevant physics and is not just a curve-fitting exercise. A better test is to apply it to an independent data set. One study which has a significantly different initial volume is the full scale Thorney Island dispersion study [12]. Of the several experiments carried out, Trial No. 9 is the closest to a calm, with a 10 m wind speed of 1.7 $m\,s^{-1}$. The initial volume of dense gas is several orders of magnitude larger, i.e., 2000 m^3. The Thorney Island data fit comfortably within the laboratory data (Fig. 4).

The Thorney Island data were abstracted from concentration vs. time histories at the lowest level (0.4 m) at each of several receptors directly downwind from the source. From each trace, the peak concentration and its time of arrival were selected. There was no obvious distinction between the disk and torus. At any given time the ground-level disk concentration equals or exceeds the torus concentration, since the torus concentration decays more rapidly. Due to the wind, the torus passes by the receptor much more quickly than by gravitational settling alone. Since there is insignificant concentration decay during the passage of the torus, the peak concentration will be associated with the disk. Also, since the initial decay is due primarily to self-generated turbulence rather than wind-generated turbulence, all of the Thorney Island trials fall initially along the general decay curve of Fig. 4.

A second study with significantly different initial conditions is the laboratory study of Meroney and Lohmeyer [13]. This report contains concentration decay data for clouds having much smaller initial volumes of 35, 165, and 450 cm^3. However, the peaks in each concentration vs. time trace are associated with the torus and will be plotted later with Havens and Spicer's torus data.

5. The disk concentration distribution

In the previous section, we treated the disk as if it were uniform in concentration, and as if air entrained through the top of a porous cylinder were instantly mixed uniformly throughout the volume. However, experience tells us that in the narrow vertical dimension, a smooth distribution from a maximum at the surface to zero at the upper edge is quickly established. In the radial

direction, a much longer time is required for the edge turbulence to erode away the uniform core as the disk expands outwards. The core is uniform only in the sense that its concentration is radially invariant. Such a core is evident in the solutions of complex models [25,26], wind tunnel experiments [15,27], and in some field experiments [25]. Within the core of radius R_c (Fig. 1), the concentration is assumed to be Gaussian in the vertical direction and is given by

$$C_d = C_{db} e^{-z^2/2\sigma_{zd}^2} \qquad (r < R_c) \tag{29}$$

For a radius r beyond R_c, we assume

$$C_d = C_{db} e^{-z^2/2\sigma_{zd}^2} e^{-(r-R_c)^2/2\sigma_{rd}^2} \qquad (r > R_c) \tag{30}$$

In these expressions, C_{db} is the surface or maximum concentration and is taken to be the bulk concentration of eqn. (26). The parameters σ_{zd} and σ_{rd} are the standard deviations of the concentration distributions in the vertical direction and in the radial direction, respectively. As the cylinder grows due to gravitational spreading, the edges are eroded due to motion-induced turbulence. The position of the core radius R_c marks the boundary of the central part of the cloud as yet undisturbed by the edge turbulence. The distribution of gas on the edge is assumed to be Gaussian as given by eqn. (30). If we assume that the rate of growth of the distribution width σ_{rd} is proportional to the cloud rate dR_d/dt, then

$$\sigma_{rd} = a_3(R_d - R_o) \tag{31}$$

where a_3 is a universal constant to be determined. If we now integrate eqns. (29) and (30) over r and z to determine the total mass of gas m_g in the cloud, we find that

$$m_g = C_{db}(\pi/2)^{1/2}\sigma_{zd}\pi(R_c^2 + (2\pi)^{1/2}R_c\sigma_{rd} + 2\sigma_{rd}^2) \tag{32}$$

Since $m_g = C_{db} V_d = C_{db} H_d \pi R_d^2$, then by comparison with eqn. (32), we see that

$$H_d = (\pi/2)^{1/2}\sigma_{zd} \tag{33}$$

and

$$R_d^2 = R_c^2 + (2\pi)^{1/2}R_c\sigma_{rd} + 2\sigma_{rd}^2 \tag{34}$$

Note that eqn. (32) has the correct asymptotic limits for (1) the mass of a cylinder when $t=0$ and $\sigma_{rd}=0$, and for (2) the mass of a Gaussian puff at large time when $R_c=0$.

In order to test eqn. (29) for the vertical distribution of material, and to estimate the disk height H_d (or σ_{zd}), we compare the predictions of eqn. (29) to the data which were measured at heights of 0.6, 1.3, 2.0, and 4.0 cm [11]. The expression for surface (or bulk) concentration C_{db} was established in Section 4. The parameter a_7 is used to control the size of R_d which in turn controls H_d through the relation $V_d = \pi R_d^2 H_d$.

By examining the means and standard deviations of $r = C_{mod}/C_{obs}$ at the various heights, the best fit occurred for a value of $a_7 = 0.94$. The scatter in the model-data comparison as a function of height is shown in Fig. 5. The value of σ_{zd} used to nondimensionalize the height is calculated from eqn. (33). Most of the points which cluster around $z/\sigma_{zd} = 0.3$ are the points of lowest measurement ($z = 0.6$ cm). Hence their scatter in the ordinate direction is not due to an inadequate model of the vertical distribution but is a measure of the model's uncertainty in calculating the surface concentration (Section 4). As the abscissa increases, the scatter increases somewhat but the mean ordinate value remains close to unity, suggesting that the Gaussian model is reasonable. For the receptors beyond the lowest level, the mean and SD of the ratio r are 1.05 ± 0.59. Referring back to Section 4, we see that the mean and SD of r for the ground level receptors were 1.04 ± 0.31.

With a_7 determined, both R_d and H_d (and σ_{zd}) are quantified. The modelled cloud height σ_{zd} is plotted in Fig. 6 as model 1. The non-dimensional height falls from a value of order unity to a much smaller constant value. The disk height variation described as model 2 results from a different choice of calibration parameters and is discussed in Section 8. Torus height and peak concentration are unaffected by these parameter changes.

The remaining unknown parameter in the above equations is a_3 in eqn. (31). In eqn. (34), we have a relation among R_d, R_c, and σ_{rd}. R_c is the radius of the core region within which the concentration is invariant with r. As an expanding cloud passes over a receptor, the concentration will increase gradually, reach a maximum when the receptor distance equals R_c, and decay thereafter as top entrainment continues. The peak concentrations C_{dp} which were abstracted

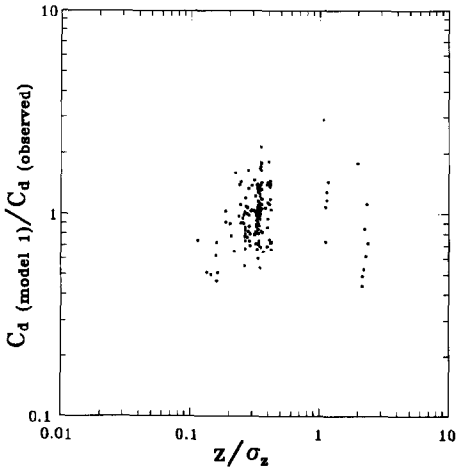

Fig. 5. The ratio of modelled to measured concentrations within the disk at various elevations (data from havens and Spicer [11]).

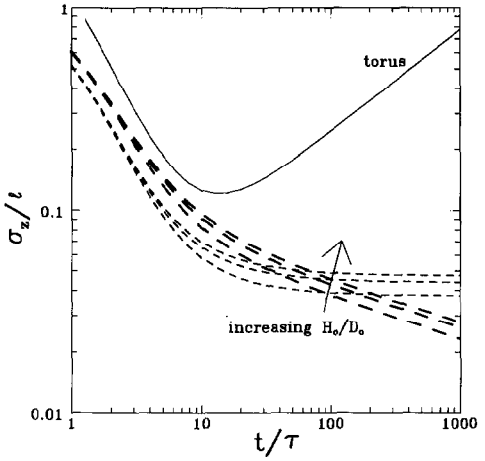

Fig. 6. The modelled variation of torus height and disk height as a function of time: $H_o/D_o = 0.4$, 1.0, 1.57. Solid curve torus; --- Model 1 disk; - - Model 2 disk.

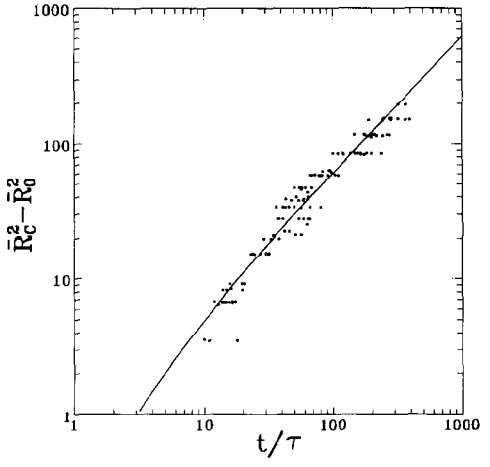

Fig. 7. The growth of the core radius within the disk as a function of time using Model 1. Solid curve from eqn. (34); ● data from Havens and Spicer [11].

from the data should therefore mark the arrival of R_c. Since the time of arrival t_{dp} is known, we can plot R_c vs. t (Fig. 7). The modelled value of R_c is derived from the quadratic expression of eqn. (34). Using eqn. (31), a value of $a_3 = 0.21$ provides the best fit. An alternate and preferable method for determining a_3 will be discussed in Section 8.

6. The torus box model

When the uniform cylinder of gas is released, radial motion is greatest at the bottom where the hydrostatic pressure is largest. This portion of the cloud forms the leading torus, having a circulation upward at the front and rearward at the top. We assume that the disk and torus separate immediately and that they grow independently of each other thereafter.

The purpose of the torus box model is to predict a bulk concentration C_{fb}. The most useful bulk concentration is one which is equal to the torus maximum surface concentration. Maximum concentrations C_{fp} were abstracted for each receptor at heights of 0.6, 1.3, 2.0, 3.0, 4.0, 6.0, 8.0, 11.0, and 16.0 cm [11]. The data at 0.6 cm were used to calibrate the box model estimate of maximum concentration; the data at higher elevations were used to estimate the height of the torus and to evaluate the efficacy of the Gaussian in describing the vertical concentration distribution.

The torus is represented as an annulus having a rectangular cross-section of height H_f, width W_f, and outer radius R_f (Fig. 1). Assuming that W_f is much smaller than R_f, the torus volume is given by

$$V_f = 2\pi R_f W_f H_f \tag{35}$$

If we make the assumption that dW_f/dt is proportional to the turbulence speed q which in turn is proportional to dR_f/dt, and that the dominant air entrainment is through the top with a velocity v_{tf} similarly proportional to the front velocity dR_f/dt (Section 3), then

$$W_f = a_6 R_f \tag{36}$$

$$v_{tf} = a_5 \frac{dR_f}{dt} \tag{37}$$

where a_5 and a_6 are proportionality constants. The rate of volume increase is given by

$$\frac{dV_f}{dt} = 2\pi R_f W_f v_{tf} \tag{38}$$

which readily integrates to become

$$\bar{V}_f = \frac{V_f}{V_{fo}} = 1 + \frac{2\pi a_5 a_6 V_o}{3V_{fo}} (\bar{R}_f^3 - \bar{R}_o^3) \tag{39}$$

where V_{fo} is the initial volume of the torus. We are assuming that it is a constant fraction of the initial cylinder volume V_o. This fraction must be solved for along with the parameters a_5 and a_6. The equation for the bulk concentration is simply the inverse of eqn. (39), i.e.,

$$\bar{C}_{fb} = C_{fb}/C_o = V_{fo}/V_f \tag{40}$$

When this modelled bulk concentration is compared to the measured surface concentrations C_{fp} of Havens and Spicer, the numerical value of the parameter group which gives the best fit is $a_5 a_6 V_o/V_{fo} = 0.018$. The fit is measured by the mean and standard deviation (SD) of the ratio $r = C_{mod}/C_{obs}$. These are 1.04 ± 0.32 over all data points. Equation (40) and the experimental data C_{fp}/C_o for $z = 0.6$ cm are plotted in Fig. 8.

As an independent check on the model, we can use the laboratory data of Meroney and Lohmeyer [13] for zero wind conditions. In their Table 4, they present peak concentrations and times of occurrence for receptors at several different radial locations. The receptors are located at a height of 2 mm, and at radial distances of 5 to 80 cm from the release point. The release volumes are small: 35, 165, and 450 cm^3. The peaks are associated with the arrival of the torus, at least for the nearby receptors, and are in reasonable agreement with the other data in Fig. 8. For the more remote receptors, we would expect the peak concentrations to be associated with the more slowly decaying disk. However, the disk is thin enough that molecular diffusion is probably significant in the vertical direction, causing disk concentrations also to fall more rapidly. Certainly the small values of $\bar{t}_{r_*}$ in Table 1 suggest that viscous effects are important during the experiment. If all the data are now compared to eqn. (40), the mean and SD of the ratio r are 1.07 ± 0.40.

With V_f and R_f established, the height H_f can be written from eqn. (35) as

$$\bar{H}_f = \frac{H_f}{l} = \frac{V_{fo}}{V_o a_6} \frac{\bar{V}_f}{2\pi \bar{R}_f^2} \tag{41}$$

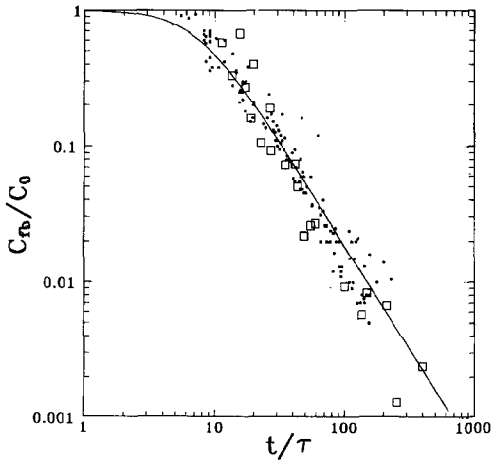

Fig. 8. The decay of the peak torus concentration as the torus is followed in time (Lagrangian mode). Solid curve from eqn. (40); ● Havens and Spicer; □ Meroney and Lohmeyer [13].

Since V_f and R_f^2 are known, the parameter group $V_{fo}/V_o a_6$ is chosen in order to have the concentration distribution in the vertical direction match the measured distribution. This is done in the next section.

7. The torus concentration distribution

Because the torus has both rotational and translational motion which cause vigorous entrainment, and because the cross-sectional dimensions are small, we assume that a Gaussian distribution is established immediately in the vertical and radial directions. Also, because the translational motion is large enough to prevent any diffusion ahead of the front, the distribution is assumed to be

$$C_f = \begin{cases} 0 & (r > R_f) \\ C_{fb} e^{-z^2/2\sigma_{zf}^2} e^{-(r-R_f)^2/2\sigma_{rf}^2} & (r < R_f) \end{cases} \tag{42}$$

for a receptor located at r, z.
If we integrate eqn. (42) over all space to find the mass m_f of the torus, we find that

$$m_f = C_{fb} 2\pi R_f (\pi/2)^{1/2} \sigma_{zf} (\pi/2)^{1/2} \sigma_{rf} \tag{43}$$

If we compare this expression with the dimensions of a bulk model, i.e.,

$$m_f = C_{fb} 2\pi R_f H_f W_f \tag{44}$$

then by comparison we find that

$$H_f = (\pi/2)^{1/2} \sigma_{zf} \tag{45}$$

$$W_f = (\pi/2)^{1/2} \sigma_{rf} \tag{46}$$

Equation (42) can now be used to examine the usefulness of the Gaussian distribution in the vertical direction, as well as to determine the height H_f (or σ_{zf}) by evaluating the parameter $V_{fo}/V_o a_6$. The peak frontal concentration data C_{fp} at all receptor heights are always located at the front of the torus, i.e., at the radius R_f. By trying to have the means of the ratios C_{mod}/C_{obs} close to unity at all receptor elevations, the best choice for $V_{fo}/V_o a_6$ is 3.5, using the Havens and Spicer data. This information, along with the value of the parameter group in eqn. (39) allows us to evaluate $a_5 = 0.063$. Because the torus is much higher than the disk, concentration measurements could be taken as high as 16 cm.

The ratios of modelled to observed concentrations are plotted in Fig. 9. For the same reasons mentioned in Section 4, these results are a reasonable indication of the validity of the Gaussian distribution. The bias and scatter of the ratio r (as measured by the mean and SD of r) for the receptors above 0.6 cm are 1.07 ± 0.66. The SD is twice the ground level of 0.32 (Section 6).

The height of the torus as a function of time is plotted in Fig. 6. Like the

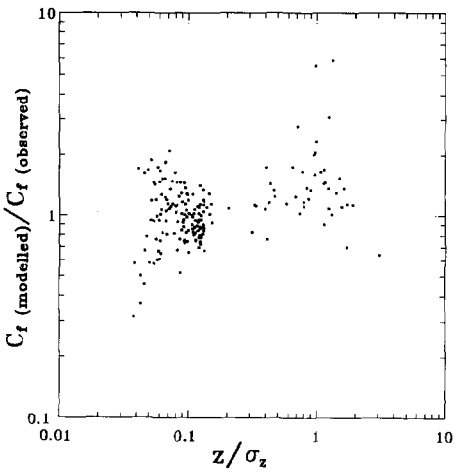

Fig. 9. The ratio of modelled to measured concentrations within the torus at various elevations (data from Havens and Spicer [11]).

disk, it collapses strongly at first but not as far. It then passes through a minimum and climbs steeply as the torus entrains air more vigorously than the disk.

8. The combined model

In Sections 4–7, we have developed concentration equations for the disk and torus. Now the two models can be combined into a dense gas puff model capable of recreating the original experiments. The model net concentration at a fixed receptor is taken as the sum of the disk and torus concentrations. Close to the source, the maximum total concentration is not allowed to exceed the initial concentration. The concentration equations, using the calibration constants developed earlier, are referred to as model 1.

The disk and torus were calibrated using a very limited and specific portion of data abstracted from a continuous set of data at each receptor. The analysis was Lagrangian in that we were following the puff from receptor to receptor, selecting only maximum concentrations. In this section, the model, constructed from single data points from numerous experiments, will be treated in an Eulerian reference frame. It will be used to predict the concentration as a function of time as the non-advecting puff spreads over a fixed receptor.

There remain two constants that require calibration using the continuous measurements at a fixed receptor. These are a_3 and a_6 and control the relative sizes of σ_{rd} and σ_{rf} respectively. Based on 4 or 5 runs with different initial conditions, reasonable values for the constants are $a_3 = 0.3$ and $a_6 = 0.15$. This

value of a_3 is more accurate than the one found in Section 4 because of the larger uncertainty in locating the time or arrival of R_c.

Figure 10(a) contains traces of 18 experiments having identical initial conditions and receptor locations. The concentrations were measured at a radius of 2 metres and at the lowest height of 0.6 cm above the laboratory floor. The initial volume, specific gravity, and height/diameter ratio were 54.1 litres, 4.19, and 1.0 respectively. The variation among the traces gives a qualitative indicator for the inherent variability in these experiments.

In an individual trace, the separation of torus and disk is usually marked by a local minimum or by a distinct change of slope. The separation is less distinct if we examine the ensemble of traces (not plotted) – a mean curve of all the traces. The ensemble curve is the logical one to compare with a mathematical solution (Model 1) which is a solution for a mean turbulent state.

In Fig. 10(a), Model 1 reproduces the early portion of the ensemble of curves fairly accurately. As the disk begins to dominate ($t>5$ seconds), the model concentration is consistently lower than the data. This is unexpected, since the model was calibrated to pass through the mean of the peak data (Fig. 4). The explanation seems to be that the disk data, abstracted as peak concentrations in the Eulerian reference frame (Fig. 2), are not peaks in the Lagrangian reference frame. In Fig. 2, the concentration C_{dp} identified as occurring at time t_{dp} is at the front edge of the expanding disk but is slightly reduced due to radial dispersion. Closer to the source and within the undisturbed core, the concen-

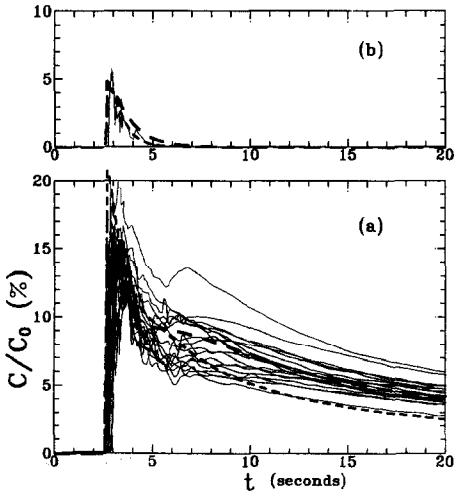

Fig. 10. Measured and modelled concentrations vs. time at two different receptor elevations z, at a radius of 2 metres (Eulerian mode). Initial conditions: $V_o=54.1$ litres, $\rho_o/\rho_a=4.19$, $H_o/D_o=1.0$ (data from Havens and Spicer [11]). (a) $z=0.6$ cm and (b) at $z=6.0$ cm: solid curves are measured data; --- Model 1 fit; - - Model 2 fit.

TABLE 2

Universal calibration constants and the equations where they first occur

	c_1	c_2	V_{fo}/V_o	a_1	a_3	a_4	a_5	a_6	a_7
Model 1	0.04	0.5	0.53	1.16	0.3	0.35	0.063	0.15	0.94
Model 2	0.07	0.4	0.7	1.16	0.35	0.35	0.063	0.2	0.8
eqn.:	(25)	(25)	(39)	(4)	(31)	(11)	(37)	(36)	(27)

tration is higher. Hence all the disk peak concentrations C_{dp} are low, becoming more so at larger times (at remote receptors where radial diffusion is larger). Consequently, the model concentration is low since it is calibrated to these data.

The data which are reliable are the original traces as in Fig. 10(a). We can qualitatively recalibrate the disk and torus equations to make a reasonable fit to these data. This is referred to as Model 2. The calibration constants are given in Table 2. With a value of $c_2 = 0.4$, the disk peak concentration falls more slowly, i.e., $C_{db} \alpha t^{-0.8}$ (Fig. 4). The disk height falls asymptotically as $t^{-0.2}$ rather than approaching a constant (Fig. 6). Finally, the composite model passes comfortably through the data at a fixed receptor as shown in Fig. 10(a).

In Fig. 10(b), there is good agreement between the data at an elevated receptor ($z = 6$ cm) and both model predictions. Only the torus contributes to the concentration since the disk is shallow. According to the model, the disk σ_{zd} is 2 cm at $t = 5$ s, and 1.4 cm at $t = 20$ s.

Model 2 was applied to several other receptors at different radial locations and showed good agreement with the concentration trace data in each case. The concentration uncertainty or standard deviation which was calculated for Model 1 should be a reasonable estimate of the uncertainty for Model 2.

Using the values of parameters and parameter groups established earlier, the initial volume of the torus V_{fo} relative to the total initial volume V_o is found to be $V_{fo}/V_o = 0.53$ for Model 1 and 0.7 for Model 2.

9. Conclusions

(1) Simple entrainment models have been a source of concern because of an apparent violation of the law of conservation of energy [5]. In such models, the cloud total energy grows indefinitely as the cloud height and radius grow. The present analysis of the Havens and Spicer data suggests that the height of the central portion (disk) decreases slowly, whereas the torus height grows continuously (at least within the range of the data). The increase in potential energy of the torus is probably fed by its rotational and radial kinetic energy. No comment can be made on the behaviour of the concentration decay in calm air for non-dimensional times beyond 400.

(2) Since the model gives reasonable results for several different experiments, it appears to be generally applicable for instantaneous dense gas releases in calm air.

(3) A cylindrical model is quite general in application, since most instantaneous releases of arbitrary shape probably tend towards such symmetry.

(4) The torus is assumed to grow independently of the trailing disk. The torus entrains material through both top and sides. As a box model, it has a rectangular cross-section. As a concentration model, it simulates a circular line source with radius R_f at height zero, having Gaussian distributions in (a) the vertical and (b) radially inwards towards the centre. The peak concentration decays as $t^{-1.5}$.

(5) The disk equations assume that all of the initial cylinder mass remains in the disk. This conservative assumption does not seem to adversely affect the model predictions. The pollutant mass transferred initially to the torus is probably returned to the disk as time progresses. The air which is entrained through the top serves to reduce the peak concentration of the disk. Edge entrainment causes the formation of a radial Gaussian distribution and tends to reduce the value of the core radius R_c. Hence both top and edge entrainment are important, but for different reasons. The peak concentration decays as $t^{-0.8}$.

(6) The Gaussian seems to be a suitable distribution for describing the concentration variation in the vertical and radial directions.

(7) The location of the leading edge of the cloud is accurate to within 5%. Surface concentration calculations are accurate to within about 30%. Concentrations measured at arbitrary heights have less accuracy. These results hold to within the non-dimensional time and space regions defined by the experiments. The concept of accuracy means that about 68% of the data would be located within one standard deviation of the model estimate (mean). This assumes that the distribution of concentrations about the mean is approximately normal.

(8) For nondimensional times greater than 100, the following approximate relations hold: $w_f = a_6 R_f \simeq 0.2R_f$; $H_f \simeq a_5 R_f \simeq 0.063R_f$; $\sigma_{rf} \simeq W_f \simeq 0.2R_f$; $R_d \simeq a_7 Rf \simeq 0.8R_f$; $\sigma_{rd} \simeq a_3 R_d \simeq 0.28R_f$; $H_d \simeq 0.13\bar{t}^{-0.2}$; $R_f \simeq \bar{t}^{0.5}$.

(9) The choice of r and $\log r$ as statistical variables is very useful in estimating error bounds on model estimates. Error estimates will be examined in a future study using a more practical model for calculating dispersion in non-zero winds.

References

1 C.J. Wheatley and D.M. Webber, Aspects of the dispersion of denser-than-air vapours relevant to gas cloud explosions, Report No. EUR 9592 EN, Commission of the European Communities, Brussels, 1984.

2 A.P. van Ulden, On the spreading of a heavy gas released near the ground, In: C.H. Buschman (Ed.), Proceedings of the 1st International Loss Prevention Symposium, The Hague, Elsevier, Amsterdam, 1974.

3 A.E. Germeles and E.M. Drake, Gravity spreading and atmospheric dispersion of LNG vapour clouds, In: Proceedings of the 4th International Symposium on the Transport of Hazardous Cargoes by Sea and Inland Waterways, Jacksonville, 1975, NTIS No. AD/A-023 505, pp. 519–539.

4 J.A. Fay, Gravitational spread and dilution of heavy vapor clouds, In: T. Carstens and T. McClimans (Eds.), Proceedings of the 2nd International Symposium on Stratified Flows, Tapir Publ., Trondheim, 1980, pp. 471–494.

5 J.A. Fay and D.A. Ranck, Comparison of experiments on dense cloud dispersion, Atmos. Environ., 17 (1983) 239–248.

6 J.A. Fay and S.G. Zemba, Modeling the dispersion of initially compact dense gas clouds, In: J. Woodward (Ed.), Proceedings of International Conference on Vapor Cloud Modeling, Cambridge, MA, 1987, pp. 439–452, Am. Inst. Chem. Eng., New York, NY.

7 D.M. Webber and C.J. Wheatley, The effect of initial potential energy on the dilution of a heavy gas cloud, J. Hazardous Materials, 16 (1987) 357–380.

8 A.P. van Ulden, A new bulk model for dense gas dispersion: Two dimensional spread in still air, In: G. Ooms and H. Tennekes (Eds.), Atmospheric Dispersion of Heavy Gases and Small Particles (IUTAM proceedings), Springer Verlag, Berlin, 1984, pp. 419–440.

9 A.P. van Ulden, The spreading and mixing of dense gas clouds in still air, Prepared for: Koninklijk Nederlands Meteorologisch Instituut, Report No. WR87-12, De Bilt, 1987.

10 A.P. van Ulden, The heavy gas mixing process in still air at Thorney Island and in the laboratory, J. Hazardous Materials, 16 (1897) 411–425.

11 J.A. Havens and T.O. Spicer, Laboratory calm air heavy gas dispersion experiments, (Development of an atmospheric dispersion model for heavier than air gas mixtures, Vol. II), US Coast Guard Report CG-D-23-85, 1985.

12 J. McQuaid, Objectives and design of the Phase I heavy gas dispersion trials. J. Hazardous Materials, 11 (1985) 1–33. NTIS No. PB 85-228633/GAR.

13 R.N. Meroney and A. Lohmeyer, Gravity spreading and dispersion of dense gas clouds released suddenly into a turbulent boundary layer, Prepared for: Gas Research Institute, Contract No. 5014-352-0203, (Chicago, IL, 1982).

14 D.J. Hall, E.J. Hollis and H. Ishaq, A wind tunnel model of the Porton dense gas spill field trials, Report no. LR 394 (AP), Stevenage (U.K.) 1982.

15 M.E. Davies and P.N. Inman, Wind tunnel modelling of the Thorney Island heavy gas dispersion trials, For: Gas Research Institute, Contract No. 5084-252-1016, 1986.

16 D.M. Webber, The physics of heavy gas cloud dispersal, UKAEA Report SRD R 243, Safety and Reliability Directorate, Culcheth, Warrington (U.K.), 1983.

17 H.E. Huppert and J.E. Simpson, The slumping of gravity currents, J. Fluid Mech., 99 (1980) 785–799.

18 R.E. Britter, Atmospheric dispersion of dense gases, Ann. Rev. Fluid Mech., 21 (1989) 317–344.

19 J.E. Simpson, Gravity currents in the laboratory, atmosphere, and ocean, Ann. Rev. Fluid Mech., 14 (1982) 213–234.

20 J.E. Simpson, Gravity currents in the environment and in the laboratory, Ellis Horwood, Chichester, 1987.

21 G.L. Mellor and T. Yamada, A hierarchy of turbulence closure models for planetary boundary layers, J. Atmos. Sci., 31 (1974) 1791–1806.

22 A. Venkatram, Topics in applied dispersion modelling, In: A Venkatram and J.C. Wyngaard (Eds.), Lectures on Air Pollution Modelling, Am. Met. Soc., Boston, MA, 1988, p. 312.

23 R.N. Meroney and A. Lohmeyer, Statistical characteristics of instantaneous dense gas clouds released in an atmospheric boundary layer wind tunnel. Boundary Layer Meteorol., 28 (1984) 1–22.

24 D.J. Hall, E.J. Hollis and H. Ishaq, A wind tunnel model of the Porton dense gas spill field trials, In: G. Ooms and H. Tennekes (Eds.), Atmospheric Dispersion of Heavy Gasea and Small Particles, Springer Verlag, Berlin, 1984, pp. 189-210.
25 D.L. Ermak, S.T. Chan, D.L. Morgan and L.K. Morris, A comparison of dense gas dispersion model simulations with Burro series LNG test results, J. Hazardous Materials, 6 (1982) 129-160.
26 R.N. Meroney, Transient characteristics of dense gas dispersion Part I: A depth-average numerical model, J. Hazardous Materials, 9 (1984) 139-157.
27 R.E. Britter, A review of some mixing experiments relevant to dense gas dispersion, In: J.S. Puttock (Ed.), Stably Stratified Flow and Dense Gas Dispersion, Clarendon Press, Oxford, 1988, pp. 1-38.